Charging Dirac States at Antiphase Domain Boundaries in the Three-Dimensional Topological Insulator Bi_{2}Se_{3}

Y. Liu, Y. Y. Li, D. Gilks, V. K. Lazarov, M. Weinert, and L. Li

Phys. Rev. Lett. **110**, 186804 — Published 1 May 2013

DOI: 10.1103/PhysRevLett.110.186804

Charging Dirac states at anti-phase domain boundaries in the three-dimensional topological insulator Bi_2Se_3

Y. Liu[1], Y. Y. Li[1], D. Gilks[2], V. K. Lazarov[2], M. Weinert[1], and L. Li[1]*

[1]Department of Physics, University of Wisconsin, Milwaukee, WI 53211, USA

[2]Department of Physics, The University of York, York, YO10 5DD, UK

Abstract:

Using scanning tunneling microscopy and transmission electron microscopy, we demonstrate the existence of anti-phase boundaries (APBs) between neighboring grains shifted by a fraction of a quintuple layer in epitaxial (0001) films of the three-dimensional topological insulator Bi_2Se_3. Scanning tunneling spectroscopy and first-principles calculations reveal that these APBs provide electrostatic fields on the order of 10^8 V/m that locally charge the Dirac states, modulating the carrier density, and shift the Dirac point by up to 120 meV. This intrinsic electric field effect, demonstrated here near interfaces between Bi_2Se_3 grains, provides direct experimental evidence at the atomic scale that the Dirac states are indeed robust against extended structural defects and tunable by electric fields. These results also shed light on the recent observation of coexistence of Dirac states and two-dimensional electron gas on Bi_2Se_3(0001) after adsorption of metal atoms and gas molecules.

PACS: 68.37.Ef, 73.20.-r, 68.37.Ma, 61.72.Nn

*lianli@uwm.edu

Crystalline solids generally consist of microscopic crystal grains joined by boundaries, where the mismatch between neighboring grains is typically accommodated by perturbation of the regular arrangement of atoms [1]. As such, grain boundaries (GBs) can have significant impact on the physical and electronic properties of the host materials, such as in the case of layered cuprate superconductors, where suprercurrents are suppressed near charged GBs [2]. In epitaxial graphene grown by chemical vapor deposition, on the other hand, GBs are found to enhance its physical strength [3,4], to act as a near perfect valley filter for valleytronics [5], and to open a transport gap for electronics [6].

The formation of GBs is also inherent in epitaxial thin films of the newly discovered three-dimensional topological insulators (TIs) Bi_2X_3 (X=Se, Te), where the spin-momentum locked surface Dirac states are being explored for applications in spintronics and quantum computing [7-12]. The layered structure of the Bi-chalchogenides, in which five atomic layers in the sequence of -X-Bi-X-Bi-X- form a quintuple layer (QL) unit along the [0001] direction, have intrinsically strong intra-layer and weak (van der Waals) interlayer bonding that facilitate a common spiral growth mode on virtually any substrates during molecular beam epitaxy (MBE) [13-22]. Coalescence of the spirals during growth results in the formation of a high density of GBs [21,22], creating inhomogeneities on the order of the grain size that could significantly modify carrier transport [23-26]. Moreover, these GBs also introduce dislocations and planar defects that allow for atomic scale studies of the predicted gapless states and other non-Abelian excitations in TIs [27-30].

In this work, using scanning tunneling microscopy (STM) and scanning transmission electron microscopy (STEM), we find that relative shifts between neighboring grains along the [0001] direction by a fraction of the Bi_2Se_3 QL lead to the formation of anti-phase domain

boundaries (APBs), i.e., zero-degree GBs, in MBE-grown Bi_2Se_3(0001) thin films. Scanning tunneling spectroscopy (STS) and density functional theory (DFT) calculations further reveal that these APBs provide electrostatic fields on the order of 10^8 V/m that locally charge the (0001) Dirac states, modulating the carrier density and shifting the Dirac point by up to 120 meV. This intrinsic electric field effect, demonstrated here at interfaces between Bi_2Se_3 grains, is similar to the surface space-charge regions in conventional semiconductor devices [31], providing direct experimental evidence at the atomic scale that the Dirac states are tunable by electric fields. In addition, these results also shed light on the recent observation of the coexistence of Dirac states and two-dimensional electron gas on $Bi2Se_3$(0001) after adsorption of gas molecules and metal atoms [32-38].

Bi_2Se_3 films were grown on epitaxial graphene/SiC(0001) at 275-325 ^oC. Bi and Se are supplied via separate Knudsen cells at 460 and 250 ^oC, respectively [22,39]. The Se/Bi ratio and substrate temperature were varied to control the density of spirals and GBs. STM images were taken at room and liquid nitrogen temperatures using electrochemically etched polycrystalline W tips, or mechanically sharpened Pt tips with the bias voltage applied to the sample. The dI/dV spectra were acquired by turning off the feedback loop, applying a small a.c. modulation of 12 mV at 860 Hz to the bias voltage, and measuring the corresponding changes in tunneling current by lock-in detection. High angle annular dark field (HAADF) imaging was carried out by STEM, and simulations of model grain boundaries and interfaces were done using a multislice image simulation approach as implemented in the 'jems' electron microscopy software [40]. Cross-section TEM specimens were prepared by conventional methods described elsewhere [41].

Figure 1(a) presents the typical morphology of Bi_2Se_3 thin films studied in this work, all of which exhibit triangular growth spirals with edges often mis-aligned, as indicated by the two

dashed lines in Fig. 1(a). Depending on growth conditions, coalescence of these spirals during growth leads to the formation of GBs (one marked by an arrow) at a density of ~ 10^9/cm^2, and with in-plane rotation ranging from 0 to 23^o between neighboring grains. In this work, we focus on the atomic and electronic structures of the zero-angle GBs (Fig. 1(b)), which accounts for ~7% of the total GBs [42]. Close analysis of the image and line-profile reveals that there is no relative in-plane rotation across the neighboring grains (and hence the "zero-angle"), but a vertical shift of 0.3 Å is observed.

The impact of the zero-angle GBs on the Dirac states of Bi_2Se_3(0001) is investigated by dI/dV tunneling spectroscopy, which measures the local density of states (LDOS) at the position of the STM tip. Spatially resolved spectra across the GB (marked *1-10* in Fig. 1(b)) are presented in Fig. 1(c). Away from the GB, the dI/dV spectrum exhibits a general V-shape (spectrum 1), with the conductance minimum attributed to electron tunneling to the Dirac point (E_D) [22,43-44]. In this case, the Dirac point is at 300 meV below the Fermi level (E_F), indicating that the Bi_2Se_3 film is n-doped due to the Se vacancies typically present in MBE grown materials [22,43-44]. Moving closer to the GB, the Dirac point shifts to more negative values and the tunneling conductance at E_F gradually decreases, leading to a W shape right at the interface with E_D at -420 meV (spectrum 5). Crossing over to the other side of the boundary, E_D shifts back towards E_F where the tunneling conductance also gradually increases. Eventually, the spectrum returns to the single V shape (spectrum 10) at about 2 nm away from the GB. Clearly, the Dirac point is present in all spectra, demonstrating at the atomic scale that the (0001) Dirac states are robust against extended structural disorders.

The shift of E_D relative to E_F indicates variations in carrier concentrations near the GB, which can be estimated by $n=\pi E_D^2/(hv_F)^2$, where v_F is the Fermi velocity [12,45]. Taking a value

of $5x10^5$ cm/s for v_F from angle-resolved photoemission spectroscopy (ARPES) studies [9], the carrier concentrations are plotted in Fig. 1(d). The spatial variations of the carrier concentrations (~$5.0x10^{12}$ cm^{-2}) observed here suggest accumulation of electrons near these zero-angle GBs in Bi_2Se_3(0001), similar to the space charge regions in conventional semiconductors [31].

Since GBs are extended defects originating from the bulk, cross-sectional atomic resolution HAADF imaging were carried out to determine their atomic structure. Shown in Fig. 2(a) is a region where two grains oriented along the [11-20] direction intersect. In the HAADF imaging mode, the large-angle elastically scattered electrons are collected by a high-angle annular detector with acceptance angle in the range of 75-170 mrads, where scattered electrons are sensitive to ~Z^2; thus the bright (dim) dots correspond to the Bi (Se) atomic columns. Close inspection of the images reveals that even though the two grains coalesce with no rotational mismatch, only half of the Bi planes are in registry between the grains, while the other half converge with the Se planes (indicated by arrows in Fig. 2(a)), resulting in an APB, likely formed due to the nucleation of two Bi_2Se_3 grains on substrate steps with heights differing by a fraction of the Bi_2Se_3 unit cell in the [0001] direction [22]. A step height of ~3/5 QL (Fig. 2(b)) could provide the relative shift between the *A1* and *A2* grains observed here. The experimental image in Fig. 2(a) also indicates that while the intensity of continuous Bi atomic planes do not change across the APB, the out-of-registry Bi planes in fact show a decrease in contrast. This reduction of intensity is not reproduced by the calculated image of edge-on APB constrained to the (10-10) plane (Fig. 2(c)), but can be generated by the introduction of a small tilt in the model, e.g., ~ 5° tilt off the [11-20] direction (Fig. 2(c) & inset in Fig. 2(a)). This confirms that the intensity change of the out-of-registry Bi columns across the APB is a geometrical effect, caused by projection overlap of Bi and Se atomic columns.

To address how these APBs modify the electronic properties, DFT calculations of two models (Figs. 3(a) and (b)) corresponding to shifts of ±3/5 of a QL were carried out. These shifts (as well as shifts of ±6/5) maintain the ABC stacking, thereby avoiding unrealistically short interatomic separations at the interface that will occur for other shifts. We focus on the ±3/5 shifts since these (but not the ±6/5 ones) have Bi layers that extend across the interface, as seen experimentally (cf., Fig. 2). The interfaces of Bi_2Se_3 were modeled using 90 atom cells consisting of 18 atomic layers perpendicular to the interface, such that the interfaces are separated by ~21.5 Å. The APBs were formed by rigidly shifting the (bulk-relaxed) structures by ±3/5 of a QL height; no attempt was made to further relax the atoms. The relativistic calculations were performed using the Full-potential Linearized Augmented Plane Wave (FLAPW) method as implemented in *flair* [46]. The wave functions and density/potential cutoffs were 218 and 1960 eV, respectively, and a 32×4×6 k-point mesh was used. For the reference (0001) surface, calculations using comparable computational parameters for 8-14 QLs were performed, with the separation between the centers of the QLs fixed at the nominal c/a value of 2.307 (a=4.138Å). The self-consistent electron densities and Coulomb potentials were planar-averaged perpendicular to the interfaces, and then the values of the central layers were subtracted to obtain the shifts corresponding to the interface. In the band structure plots, the states were weighted by their spatial localization at the interface.

While both structures are stoichiometric (Fig. 3), they differ in how the discontinuous layers are connected (indicated by ovals), i.e., the number (1 or 2) of Bi-Bi or Se-Se links per 3 QL. The APB formation energy is ~ 32 meV/Å^2 for the "1 Se-Se + 2 Bi-Bi" interface (+3/5 QL variant, also Fig. 2), with the "2 Se-Se + 1 Bi-Bi" (-3/5 QL) variant only slightly less stable (by ~ 1 meV/Å^2); the ±6/5 QL interface formation energies are ~3 times larger. Because the outer Se

atoms of the relaxed bulk QLs are shifted inward, the continuous Se layers have a height difference of ~0.3 Å across the interface, in excellent agreement with STM observations (Fig. 1(b)). In both cases the interface is charged (compared to "bulk" regions away from the interface), as shown in Fig. 3(c), albeit with opposite signs. These localized charges result in changes in the planar-averaged Coulomb potential (Fig. 3(d)) of the order of 0.2 eV within about 1 nm of the interface: a decrease (increase) of the electronic density at the interface results in an attractive (repulsive) potential/electric field; similar behavior is seen for the ±6/5 variants. These changes to the potential will in turn shift the surface states – including the Dirac states – on the (0001) surface (Fig. 3(e)) in the vicinity of the APBs. In particular, the decrease in electronic density relative to "bulk" values at the "1 Se-Se + 2 Bi-Bi" interface (corresponding to $\sim 0.8\times10^{13}$ cm^{-2} in the first peak) will shift the Dirac state to greater binding energy, resulting in a compensating increased electronic carrier density at the surface, in excellent agreement with tunneling spectroscopy observations (Fig. 1(d)). These calculated Coulomb potential changes indicate an effective electric field of $\sim 10^8$ V/m.

The charging (and potential shifts) in the vicinity of the GB are the result of the formation of interface states. Comparing the bulk bands along Γ-K, projected perpendicular to the interface (Fig. 3(f)), both interfaces (Figs. 3(g) and (h)) have (metallic) interface states in the gap. In Fig. 3g (3h) the bands localized at the interface are above (below) the Fermi level, corresponding to a loss (gain) of electrons. In both cases, there are compensating states with their weight further away from the interface. All these interface states are "normal" – there are *not* topological interface states since the bulk materials on both sides of the interface have the *same* (non-trivial) Z_2 invariant – i.e., they are fully within the gap, can shift so not to cross the Fermi level, have the

same band topology with and without spin-orbit, and are not spin-momentum locked; the degeneracies seen in Figs. 3(g,h) are dictated by the crystal symmetry in the standard manner.

The tunneling spectra observed near the charged GBs in Bi_2Se_3 films can now be understood within a band bending model [31], in which electrostatic fields in the vicinity of the interface cause rigid shifts of both the bulk and surface state bands. For finite number of QLs – e.g., 8 QLs as shown here (Fig. 4) – the calculated valence and conduction bands are comprised of quantum well (QW) states, where the number of these states in the bands (7) is equal to the number of QLs minus one due to the formation of the Dirac state. The calculated band widths, i.e., edges of both the valence and conduction bands, are the same for 8-14 QL since they are determined by the interaction between the QLs. Away from the GB, the rapid increases of the tunneling conductance above E_F and below E_D are due to the contributions from the bottom of conduction band and top of the valence band, respectively (left panel, Fig. 4). Near the GBs, the attractive electrostatic potential causes downward band bending at the surface, moving the conduction band edge to below E_F. Because of the lower DOS away from the conduction band edge, there is a decrease in the tunneling conductance at E_F (right panel, Fig. 4); in addition, the interface states may also be responsible for features in the spectra at the GB itself (cf., line 5 in Fig. 1(c)). Note that the Dirac points shift relative to E_F, but not significantly relative to the band edges, because the predominant effect of the zero-angle GB is to provide an additional electrostatic potential, in excellent agreement with the experiment.

These results also shed light on the recent observations of the coexistence of Dirac states and a two-dimensional electron gas on $Bi_2Se_3(0001)$ after adsorption of gas molecules and metal atoms [32-38]. Our model suggests that the charging due to the adsorbates cause a downward band bending, making the (QWs) states in the conduction bands accessible to ARPES

measurements. Depending on the nature of interactions with the adsorbate, the position of the Dirac point relative to the band gap edges may also change. A consequence is that in the case of adsobates (e.g., an "aged" surface), potential variations across the surface are expected, resulting in local variations in the energy of the Dirac states (c.f., Fig. 1d) [47], thus causing an energy broadening of the states.

In summary, we determine the atomic structure of zero-angle GBs in MBE-grown Bi_2Se_3(0001) thin films, and show that interfaces between neighboring grains do not host topological states. We further find that these GBs are charged, and significantly modify the Dirac states nearby. Although the GBs observed here, both with TEM and STM/STS, were of the +3/5 QL type with an attractive electrostatic potential, growth of the other variants should be possible by choice of substrates with different step morphology. The control of Dirac states, demonstrated here near Bi_2Se_3 grain boundaries at the atomic scale, provides direct experimental evidence that Dirac states are indeed robust against extended structural defects and are tunable by electric fields, key to enable applications in electronic devices.

Acknowledgement: Funding for this work was provided by NSF (DMR- 1105839).

Figure captions:

Figure 1 (a) STM image of triangular growth spirals on a 50 nm Bi_2Se_3 film (V_s=0.56 V, I_t=0.1 nA). (b) Atomic resolution image of a zero-angle GB (V_s=-0.2 V, I_t=1.0 nA), and line-profile along the marked line. (c) Spatially resolved dI/dV spectra taken across the GB at positions marked *1-10* in (b). (c) Dirac point energies and corresponding carrier concentrations across the GB at positions *1-10.*

Figure 2 (a) HAADF cross-sectional image of a Bi_2Se_3 film showing the APB between two coalesced grains (A1 and A2) that are shifted ~3.8 Å along the growth direction. (b) A model of edge-on APB in the [11-20] direction, and the corresponding simulated HAADF image. Green (blue) filled circles represent Bi (Se). (c) Simulated HAADF image of the APB model with ~ 5º tilt off the [11-20] direction, also shown as inset in (a).

Figure 3 Interface models distinguished by the number of Se-Se and Bi-Bi "links" connecting Bi rows per 3 QLs: (a) "1 Se-Se + 2 Bi-Bi", and (b) "2 Se-Se + 1 Bi-Bi". Planar-averaged densities (c), and Coulomb potentials (d), compared to the corresponding values in the middle ("bulk") of the material for the two models shown in (a) & (b). Red dots denote the positions of the atomic planes. (e) Calculated bands for the (0001) surface of a 8 QL film, showing the Dirac state (arrow). (f) Calculated bulk bands projected perpendicular to the interfaces, [01-10], onto the Γ-K line. The apparent symmetry line at ¾ Γ-K is due to states at a bulk M point, which is a time reversal invariant point. (g) & (h) Calculated bands, weighted by the spatial localization of the wave functions in the interface region for the "1 Se-Se + 2 Bi-Bi" and "2 Se-Se + 1 Bi-Bi" interfaces, respectively.

Fig. 4 Experimental local density of states of a Bi_2Se_3 film and a n-type GB, compared to the calculated bands for 8 QL along Γ and ±1/5 K (~0.2 $Å^{-1}$), weighted by the spatial localization of the states above the surface. The energy scales of the experiments and calculations are the same, but with the calculations shifted to align the Dirac energy E_D. Note that Dirac point in tunneling spectra could be shifted by the tip-induced band bending [43], which is not included here.

References:

1. J. P. Hirth and J. Lothe, Theory of dislocations, 2nd edition, John Wiley &Sons, 1982.
2. S. Graser, P. J. Hirschfeld, T. Kopp, R. Gutser, B. M., Andersen, and J. Mannhart, Nature Phys. **6**, 609 (2010).
3. R. Granta, V. B. Shenoy, and R. S. Ruoff, Science **330**, 946 (2010).
4. Y. Wei, J. Wu, H. Yin, X. Shi, R. Yang, and M. Dresselhaus, Nature Mater. **11**, 759 (2012).
5. D. Gunlycke and C. T. White, Phys. Rev. Lett. **106**, 136806 (2011).
6. O. V. Yazyev and S. G. Louie, Nature Mater. **9**, 806 (2010).
7. H. Zhang, C. -X. Liu, X. -L. Qi, X. Dai, Z. Fang, and S. -C. Zhang, Nature Phys. **5**, 438 (2009).
8. D. Hsieh et al., Nature **460**, 1101 (2009).
9. Y. Xia et al., Nature Phys. **5**, 398 (2009).
10. Y. L. Chen et al., Science **325**, 178 (2009).
11. Y. Zhang et al., Nature Phys. **6**, 584 (2010).
12. M. Z. Hasan and C. L. Kane, Rev. Mod. Phys. **82**, 3045 (2010).
13. J. Chen et al., Phys. Rev. Lett. **105**, 176602 (2010).
14. C. –L. Song et al., Appl. Phys. Lett. **97**, 143118 (2010).
15. A. Richardella et al., Appl. Phys. Lett. **97**, 262104 (2010).
16. N. Bansal et al., Thin Solid Films **520**, 224 (2011).
17. L. He et al., J. Appl. Phys. **109**, 103702 (2011).
18. Z. Y. Wang, H. D. Li, X. Guo, W. K. Ho, and M. H. Xie, J. Cryst. Growth **334**, 96 (2011).

19. C. -Z. Chang et al., SPIN **1**, 21 (2011).

20. X. F. Kou et al., Appl. Phys. Lett. **98**, 242102 (2011).

21. H. D. Li et al., N. J. Phys. **12**, 103038 (2010).

22. Y. Liu, M. Weinert, and L. Li, Phys. Rev. Lett. **108**, 115501 (2012).

23. D. Kim et al., Nature Phys. **8**, 458 (2012).

24. A. A. Taskin, S. Sasaki, K. Segawa, and Y. Ando, Phys. Rev. Lett, **109**, 066803 (2012).

25. Y. S. Kim, N. Bansal, M. Brahlek, E. Edrey, and S. Oh. Phys. Rev. Lett, **109**, 116804 (2012).

26. A. A. Taskin, S. Sasaki, K. Segawa, and Y. Ando, Adv. Mater. 24, 5581 (2012).

27. Y. Ran, Y. Zhang, and A. Vishwanath, Nature Phys. **5**, 298 (2009).

28. J. C. Y. Teo and C. L. Kane, Phys. Rev. B **82**, 115120 (2010).

29. F. Zhang, C. L. Kane, E. J. Mele, Phys. Rev. B **86**, 081303(R) (2012).

30. M. Barkeshli, and X. –L. Qi, Phys. Rev. X **2**, 031013 (2012).

31. S. M. Sze, Physics of semiconductor devices. (2^{nd} edition, John Wiley & Sons, 1981).

32. M. Bianchi, D. Guan, S. Bao, J. Mi, B. B. Iversen, P. D. C. King, and P. Hofmann, Nature Commun. **1**, 128 (2010).

33. L. A. Wray et al., Nature Phys. **7**, 32 (2011).

34. P. D. C. King et al., Phys. Rev. Lett. **107**, 096802 (2011).

35. H. M. Benia1, C. Lin, K. Kern, and C. R. Ast, Phys. Rev. Lett. **107**, 177602 (2011).

36. T. Valla, Z.-H. Pan, D. Gardner, Y. S. Lee, and S. Chu, Phys. Rev. Lett. **108**, 117601 (2012).

37. C. Chen et al., Proc. Natl. Acad. Sci. U.S.A. **109**, 3694 (2012).

38. M. Koleini, T. Frauenheim, and B. Yan, Phys. Rev. Lett. **110**, 016403 (2013).

39. Y. Qi, S. H. Rhim, G. F. Sun, M. Weinert, and L. Li, Rev. Lett. **105**, 085502 (2010).

40. P. A., Stadelman, Ultramicroscopy **21**, 131 (1987).

41. Lari et al., J. Appl. Phys. **111**, 07C311 (2012).

42. Near the vicinity of the small-angle GBs ($15^{o}>\theta>0$), both the geometric and electronic properties of the Bi_2Se_3(0001) film are significantly modified due to complex rearrangements of atoms ,which will be the subject of future studies.

43. P. Cheng et al., Phys. Rev. Lett. **105**, 076801 (2010).

44. S. Kim et al., Phys. Rev. Lett. **107**, 056803 (2011).

45. M. Chen et al., Appl. Phys. Lett. **101**, 081603 (2012).

46. M. Weinert, G. Schneider, R. Podloucky, and J. Redinger, J. Phys. Condens. Matter **21**, 084201 (2009).

47. H. Beidenkopf et al., Nature Phys. **7**, 939 (2011).

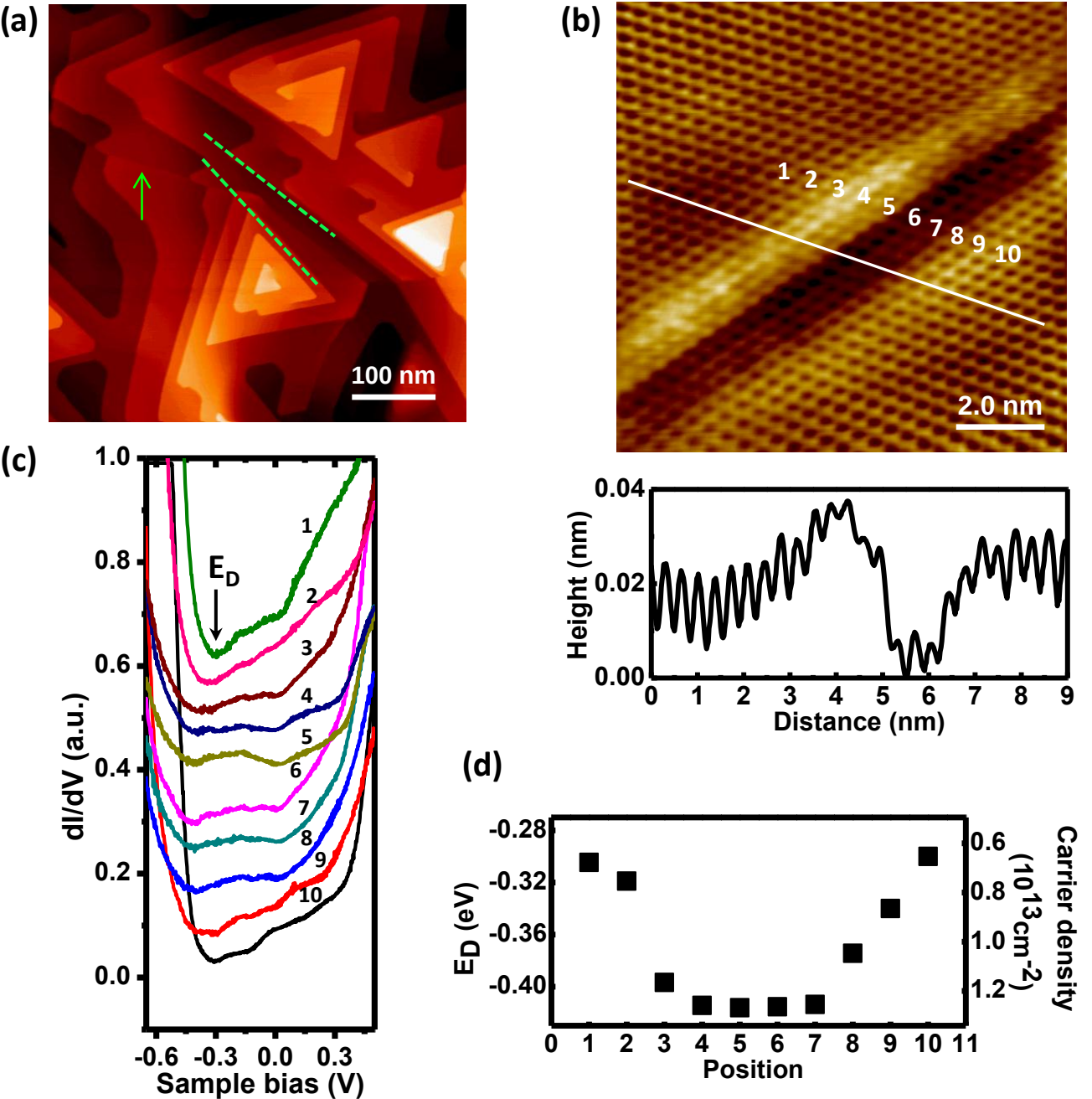
(a)
100 nm
(b)
1 2 3 4 5 6 7 8 9 10
2.0 nm
(c)
dI/dV (a.u.)
Sample bias (V)
E_D
1 2 3 4 5 6 7 8 9 10
Height (nm)
Distance (nm)
(d)
E_D (eV)
Carrier density (10^13 cm^-2)
Position

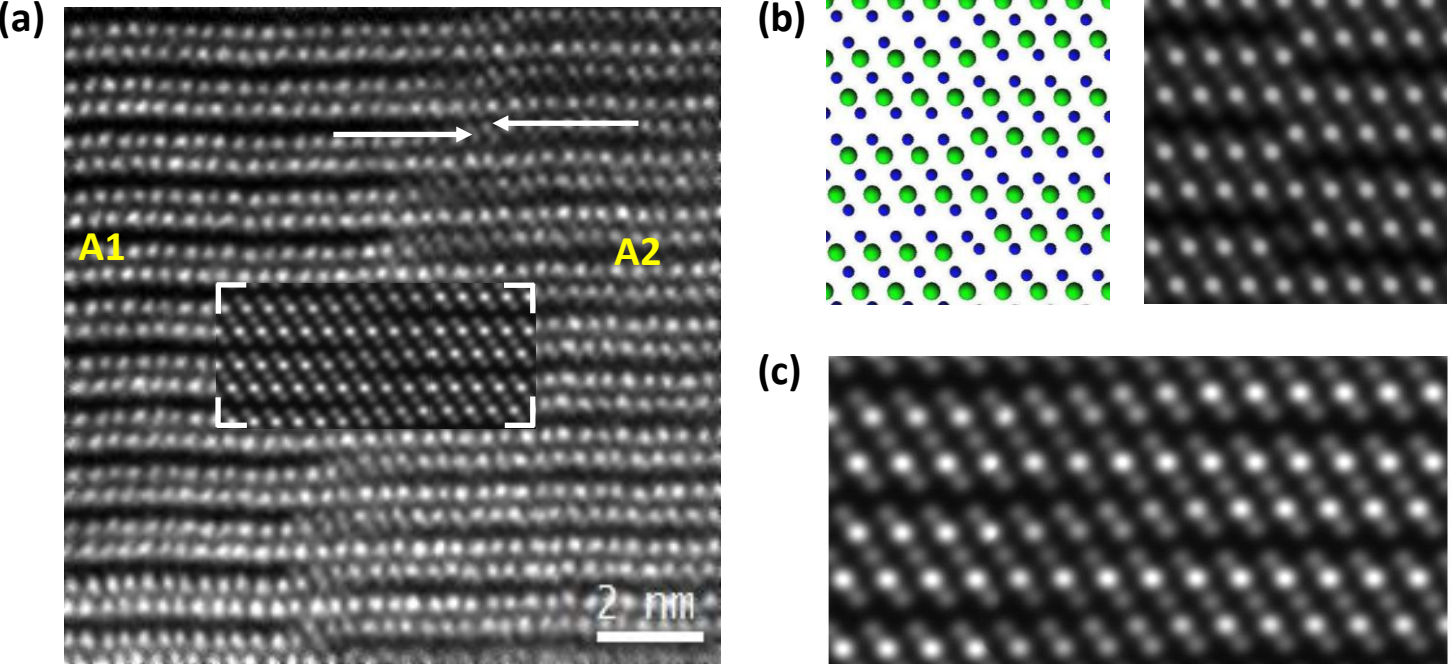
(a)
A1
A2
2 nm
(b)
(c)

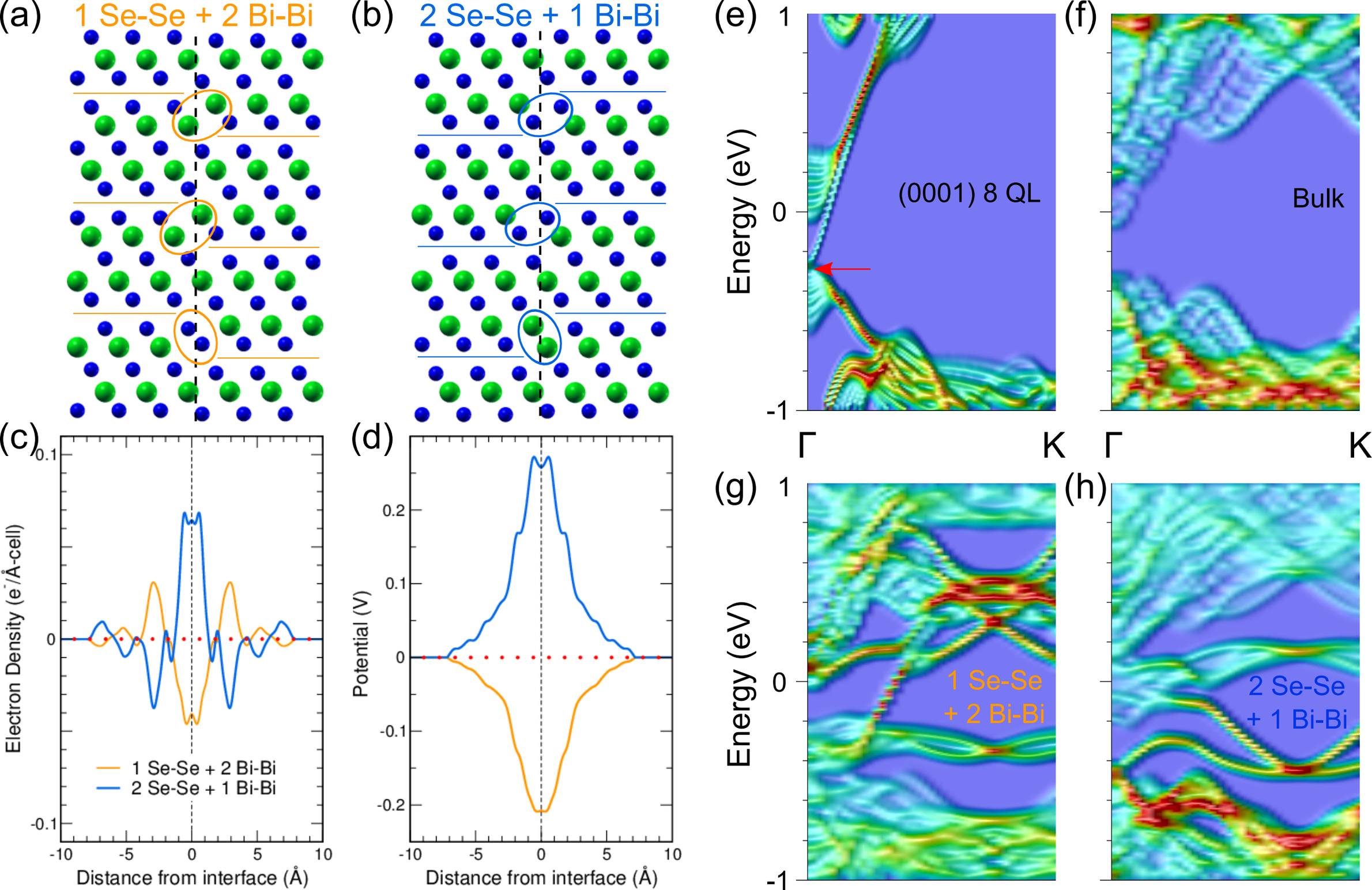
(a)
1 Se-Se + 2 Bi-Bi
(b)
2 Se-Se + 1 Bi-Bi
(c)
Electron Density (e⁻/Å-cell)
1 Se-Se + 2 Bi-Bi
2 Se-Se + 1 Bi-Bi
Distance from interface (Å)
(d)
Potential (V)
Distance from interface (Å)
(e)
Energy (eV)
(0001) 8 QL
Γ
K
(f)
Bulk
Γ
K
(g)
Energy (eV)
1 Se-Se
+ 2 Bi-Bi
(h)
2 Se-Se
+ 1 Bi-Bi

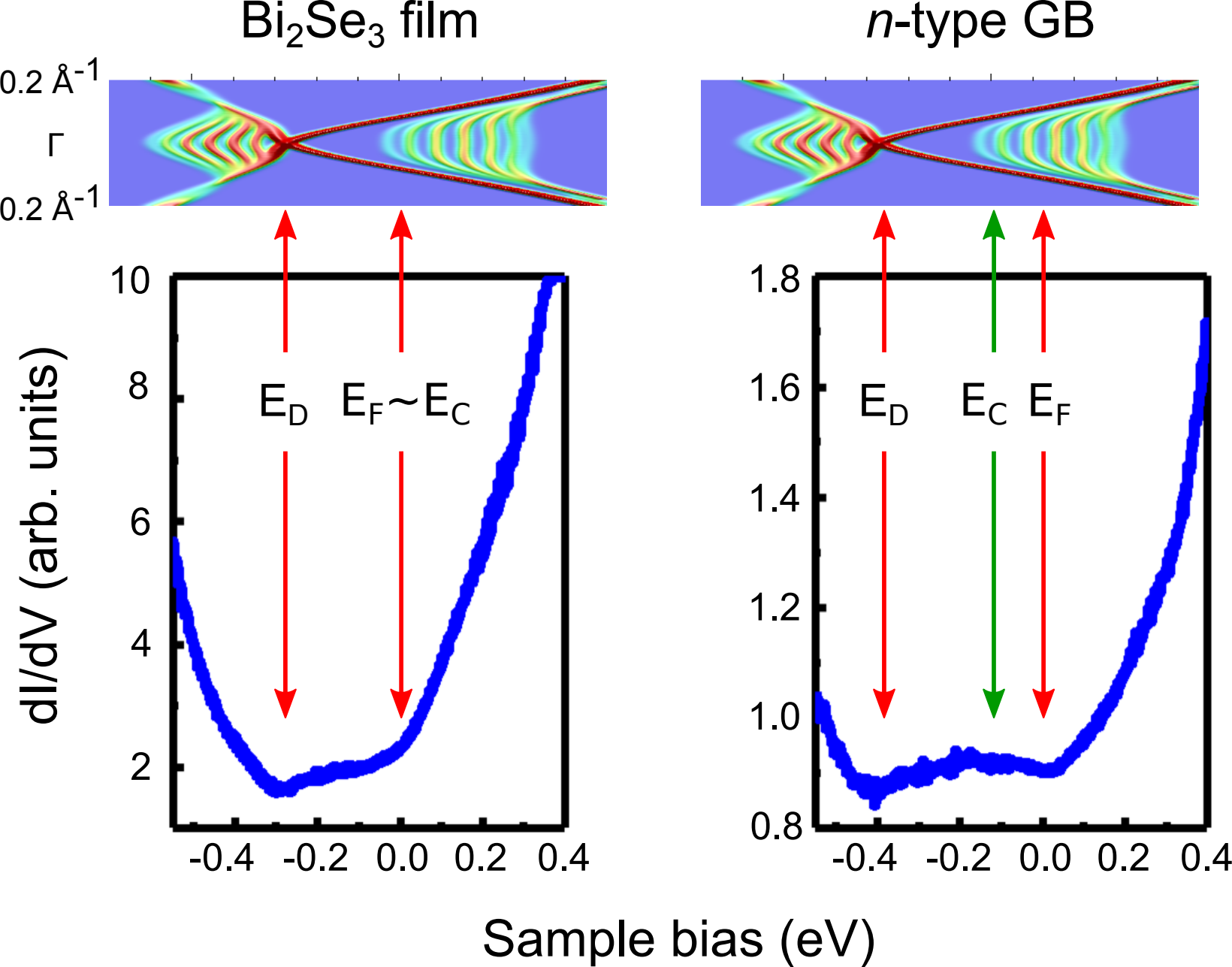
Bi2Se3 film
n-type GB
0.2 Å-1
Γ
0.2 Å-1
ED
EF~EC
EC
EF
dI/dV (arb. units)
Sample bias (eV)